THE JOURNAL OF BIOLOGICAL CHEMISTRY VOL. 290, NO. 49, pp. 29155–29166, December 4, 2015
© 2015 by The American Society for Biochemistry and Molecular Biology, Inc. Published in the U.S.A.

Structure of Human B_{12} Trafficking Protein CblD Reveals Molecular Mimicry and Identifies a New Subfamily of Nitro-FMN Reductases*

Received for publication, July 29, 2015, and in revised form, August 28, 2015 Published, JBC Papers in Press, September 13, 2015, DOI 10.1074/jbc.M115.682435

Kazuhiro Yamada[‡1], **Carmen Gherasim**[§1], **Ruma Banerjee**[§2], **and Markos Koutmos**[‡3]

From the [‡]*Department of Biochemistry, Uniformed Services University of the Health Sciences, Bethesda, Maryland 20814 and the* [§]*Department of Biological Chemistry, University of Michigan Medical School, Ann Arbor, Michigan 48109-0600*

Background: Mutations in CblD, involved in B_{12} (or cobalamin) trafficking, lead to disease.
Results: The first crystal structure of human CblD is reported.
Conclusion: CblD most closely resembles CblC, another cobalamin trafficking protein, and they belong in a new subclass with the nitro-FMN reductase superfamily.
Significance: Disease-causing mutations that impair cobalamin oxidation kinetics can now be localized on the CblD structure.

In mammals, B_{12} (or cobalamin) is an essential cofactor required by methionine synthase and methylmalonyl-CoA mutase. A complex intracellular pathway supports the assimilation of cobalamin into its active cofactor forms and delivery to its target enzymes. MMADHC (the methylmalonic aciduria and homocystinuria type D protein), commonly referred to as CblD, is a key chaperone involved in intracellular cobalamin trafficking, and mutations in CblD cause methylmalonic aciduria and/or homocystinuria. Herein, we report the first crystal structure of the globular C-terminal domain of human CblD, which is sufficient for its interaction with MMADHC (the methylmalonic aciduria and homocystinuria type C protein), or CblC, and for supporting the cytoplasmic cobalamin trafficking pathway. CblD contains an $\alpha+\beta$ fold that is structurally reminiscent of the nitro-FMN reductase superfamily. Two of the closest structural relatives of CblD are CblC, a multifunctional enzyme important for cobalamin trafficking, and the activation domain of methionine synthase. CblD, CblC, and the activation domain of methionine synthase share several distinguishing features and, together with two recently described corrinoid-dependent reductive dehalogenases, constitute a new subclass within the nitro-FMN reductase superfamily. We demonstrate that CblD enhances oxidation of cob(II)alamin bound to CblC and that disease-causing mutations in CblD impair the kinetics of this reaction. The striking structural similarity of CblD to CblC, believed to be contiguous in the cobalamin trafficking pathway, suggests the co-option of molecular mimicry as a strategy for achieving its function.

Cobalamins are B_{12} derivatives that serve as essential cofactors for two housekeeping enzymes in mammals: the mitochondrial methylmalonyl-CoA mutase and the cytosolic methionine synthase (1, 2). Following the entry of cobalamin into cells, the concerted action of several enzymes and chaperones result in the interorganellar transport, maturation, and loading of the cofactor into the active sites of its target enzymes (see Fig. 1) (3–5). Dysfunction of proteins involved in the cobalamin trafficking pathway results in either isolated or combined homocystinuria and methylmalonic aciduria, with attendant complications (6). Early clinical genetic studies on patients with inherited disorders of cobalamin metabolism led to the identification of distinct complementation groups; *cblA-G*, *cblJ*, *mut*, and *cblX* (7–15). The genes at the *cblC* and *cblD* loci encode proteins that have been named MMACHC (for methylmalonic aciduria *cblC* type, with homocystinuria) (9) and MMADHC (methylmalonic aciduria *cblD* type, with homocystinuria) (11). For simplicity, we refer to these proteins as CblC and CblD, respectively.

Both cobalamin-dependent enzymes are impaired in patients with mutations in CblC, indicating that this protein functions early in the trafficking pathway (16). In contrast, mutations in CblD can interrupt the function of either methylmalonyl-CoA mutase or methionine synthase or both enzymes (17). Consequently, patients with CblD dysfunction are classified into three distinct groups with isolated methylmalonic aciduria, isolated homocystinuria, and combined methylmalonic aciduria and homocystinuria. These clinical observations suggest that CblD functions downstream of CblC in the cobalamin trafficking pathway (see Fig. 1*A*) (17). Subcellular localization studies on CblD revealed its presence in both the cytoplasmic and mitochondrial compartments consistent with its suggested function at a branch point in B_{12} processing (18). Four missense mutations have been described in CblD that are associated with isolated homocystinuria; *i.e.* they affect only the cytoplasmic branch of the trafficking pathway. These mutations are located in the C-terminal half of CblD (see Fig. 1*B*).

CblC is predicted to be the first protein that binds cobalamin in the cytoplasm as the cofactor exits the lysosome (see Fig. 1*A*). It is a multifunctional enzyme that catalyzes a range of activities including reductive decyanation of cyanocobalamin (19) and

* This work was supported, in whole or in part, by National Institutes of Health Grant DK45776 (to R. B.). This work was also supported by American Heart Association Grant 13SDG14560056 (to M. K.). The authors declare that they have no conflicts of interest with the contents of this article.
[1] Co-first authors.
[2] To whom correspondence may be addressed. Tel.: 734-615-5238; E-mail: rbanerje@umich.edu.
[3] To whom correspondence may be addressed. Tel.: 301-295-9419; E-mail: markos.koutmos@usuhs.edu.

dealkylation of alkylcobalamins (20, 21). The activity of CblC converts cobalamins to a common cob(II)alamin intermediate, which is subsequently partitioned into the synthesis of the biologically active cofactor forms, methylcobalamin and 5′-deoxyadenosylcobalamin, required in the cytoplasm and mitochondrion, respectively. In contrast to CblC, the biological role of CblD has remained elusive. When first identified, it was speculated, based on weak primary sequence homology, to be an ATPase and/or to bind cobalamin (11). However, subsequent biochemical studies revealed that human CblD alone is incapable of binding cobalamin or hydrolyzing ATP (22, 23). So far, no ligand binding or enzymatic activity has been demonstrated for CblD. The only biochemical clue into CblD function derives from the observation that it binds to CblC, to which cob(II)alamin is bound (22–24). Based on these observations, it has been proposed that CblD serves as an adaptor protein, exerting its function in a protein-protein complex with CblC (4, 23, 25).

Progress in elucidating the function of CblD has been hampered by its lack of any obvious sequence similarity to any protein with known function and by the absence of structural information. To bridge this gap, we have solved the first crystal structure of the human protein truncated at the N terminus ($CblD^{\Delta N108}$) to remove a region that is predicted to be highly disordered. The C-terminal domain is sufficient for interaction with CblC and for supporting the cytoplasmic cobalamin-processing pathway (11, 23). We demonstrate that CblD accelerates oxidation of CblC-bound cob(II)alamin to aquocobalamin (OH_2Cbl)[4] and that missense pathogenic mutations in CblD differentially impact the kinetics of oxidation of CblC-bound cob(II)alamin. The crystal structure provides a framework for locating pathogenic mutations in CblD. Unexpectedly, the structure reveals that CblD exhibits a nitro-FMN reductase (NFR)-like fold despite the lack of sequence similarity to other family members. Within this family, CblD shares several distinguishing structural features with two other proteins involved in mammalian cobalamin metabolism, CblC, and the activation domain of methionine synthase (MS^{act}) and with two recently described bacterial corrinoid-dependent dehalogenases (26, 27). We propose that these proteins constitute a new subfamily within the NFR superfamily.

Experimental Procedures

Chemicals—Reagents used for cloning were purchased from Agilent Technologies (Santa Clara, CA) and New England BioLabs (Ipswich, MA). Tris(2-carboxyethyl) phosphine and isopropyl β-D-1-thiogalactopyranoside were from GoldBio Technology. All other chemicals were purchased from Fisher Scientific.

Cloning of CblD—$CblD^{\Delta N108}$ was cloned into a pET-28b(+) vector (Novagen) using the NdeI and XhoI restriction enzyme sites to generate the N-terminal His_6-tagged construct containing a thrombin cleavage site. Oligonucleotides containing the bases corresponding to Ser^{109}–Met^{116} (5′ β-primer) and the last 24 bases (3′-primer) of the CblD cDNA (with restriction sites underlined) were used as primers: forward, 5′-primer: 5′-CATATGAGTGAAAGAC ATGAGTTTGTGATG-3′, and 3′-primer: 5′-CTCGAGTTAATTTCCACTTAATTTCTTC-AT-3′. Construction of T182N, D246G, Y249C, and L259P pathogenic mutants of human CblD was performed using the QuikChange site-directed mutagenesis kit according to manufacturer's instructions (Agilent Technologies Inc.). The pET-28b(+) vector encoding the human CblD residues 116–296 ($CblD^{\Delta N115}$ background (23)) was used as a template with the following forward primers: 5′-ACTGTAACACAAAAAAAT-AAGATGATATGACT-3′, 5′-ACTCTTTTTGAAACTGGT-GAACGCTACCGACAT-3′, 5′-GAAACTGATAACGCTGC-CGACATTTAGGATTC-3′, and 5′-TTCTCTGTTGATGAC-CCGGGATGCTGTAAAGTG-3′ to generate T182N, D246G, Y249C, and L259P mutations. The mutagenic codons introducing asparagine, glycine, cysteine, and proline are underlined. The mutations were confirmed by DNA sequencing at the DNA Sequencing Core (University of Michigan).

Expression and Purification of CblD—Wild-type and mutant $CblD^{\Delta N115}$ and $CblD^{\Delta N108}$ proteins were expressed and purified as previously described (23). Purified protein was subjected to thrombin (GenTrac, Inc., Middleton, WI) treatment (2 units/mg protein) at 4 °C overnight, and the released His_6 tag was removed by purification through a second nickel-nitrilotriacetic acid chromatographic step. The flow-through containing the tagless $CblD^{\Delta N108}$ protein was collected and concentrated using a YM-10 (Millipore, Billerica, MA) filter and loaded onto an S200 size exclusion column (120 ml, HiLoad 16/600 Superdex 200 PG; GE Healthcare, Pittsburgh, PA) to exchange the buffer to 50 mM Tris, pH 8, containing 0.5 mM Tris(2-carboxyethyl) phosphine. The selenomethionine derivative of $CblD^{\Delta N108}$ (SeMet-$CblD^{\Delta N108}$) was expressed like the unlabeled protein with the exception that the cells were grown in minimal medium supplemented with 50 mg/liter SeMet as described previously for CblC (28).

Oxidation of CblC-bound Cob(II)alamin—Cob(II)alamin was generated by photolysis of 5′-deoxyadenosylcobalamin in a sealed anaerobic vial, and full conversion to cob(II)alamin was monitored by UV-visible spectroscopy (conversion of the 525 nm absorbance to 475 nm). An anaerobic CblC stock solution was mixed with stoichiometric cob(II)alamin (300 μM each), and excess cob(II)alamin was removed using a Nanosep 10 K centrifugal device (Pall Life Sciences, Port Washington, NY). CblC-bound cob(II)alamin oxidation was then monitored aerobically at 20 °C in 0.1 M Hepes, pH 7.4, containing 150 mM KCl and 10% glycerol. For this, the CblC-bound cob(II)alamin stock solution was added to a 150-μl cuvette containing the same but aerobic buffer to give a final solution of CblC:cob(II)alamin (30 μM bound cobalamin). For experiments containing CblD, stoichiometric amount of wild-type or T182N, D246G, Y249C, and L259P (30 μM each) CblD was added to the aerobic buffer prior to addition of CblC-bound cob(II)alamin. Oxidation of cob(II)alamin to OH_2Cbl was monitored at 525 nm and was accompanied by the decrease in the cob(II)alamin absorbance at 475 nm. Control experiments were performed by adding bovine serum albumin at 1 mg/ml to the CblC-bound cob(II)alamin solution.

[4] The abbreviations used are: OH_2Cbl, aquocobalamin; NFR, nitro-FMN reductase; MS^{act}, activation domain of methionine synthase; $CblD^{\Delta N108}$, human CblD variant in which 108 N-terminal residues are deleted; SAD, single-wavelength anomalous dispersion; AdoMet, *S*-adenosyl methionine.

Crystallization Conditions—Stock solutions of CblD$^{\Delta N108}$ (10 mg/ml) and of SeMet-CblD$^{\Delta N108}$ in 50 mM Tris, pH 8, containing 0.5 mM Tris(2-carboxyethyl) phosphine were used for crystallization trials. Crystals of both CblD$^{\Delta N108}$ and SeMet-CblD$^{\Delta N108}$ were obtained at 20 °C by the vapor diffusion method from 1:1 mixtures of protein and reservoir solution in sitting drop plates. Typical volumes of well and protein solution used for crystallization varied between 0.5 to 1.5 μl. The reservoir solutions for CblD$^{\Delta N108}$ and for SeMet-CblD$^{\Delta N108}$ contained 20% PEG3350, 0.1 M Tris-HCl, pH 7.5, 0.2 M $MgCl_2$, 0.1 M NaF (for CblD$^{\Delta N108}$), and 20% PEG3350, 0.1 M Tris-HCl, pH 7.5, 0.185 M $MgCl_2$, 0.12 M NaF (for SeMet-CblD$^{\Delta N108}$), respectively. Harvested crystals were cryo-protected by soaking in 16% PEG 3,350, 0.08 M Tris-HCl, pH 7.5, 0.16 M $MgCl_2$, 0.08 M NaF, and 20% (v/v) glycerol for a few minutes prior to flash cooling in liquid nitrogen. Crystals of CblD$^{\Delta N108}$ were of space group $P2_1$ (a = 47.6 Å, b = 67.1 Å, c = 66.2 Å, and β = 110.5°) with two molecules in the asymmetric unit (Matthews' coefficient VM = 2.3 Å^3/Da for two molecules per asymmetric unit, 46.8% solvent content). Crystals of SeMet-CblD$^{\Delta N108}$ were of space group I222 (a = 65.3 Å, b = 66.2 Å, c = 71.8 Å) with one molecule in the asymmetric unit (Matthews' coefficient VM = 1.8 Å^3/Da for one molecule per asymmetric unit, 32.2% solvent content). Detailed crystallographic information regarding data processing and refinement statistics is provided in Table 1.

X-ray Diffraction and Data Analysis—Diffraction data were collected at 100 K on Beamline GM/CA-CAT 23-ID-B at the Advanced Photon Source, Argonne National Laboratory (Argonne, IL). The data were recorded on a Mar300 detector and processed with HKL2000 (29). Phenix AutoSol (30) was used to identify the selenium sites and calculate density-modified 2.31 Å experimental maps based on a single-wavelength anomalous dispersion (SAD) data set from one SeMet-CblD$^{\Delta N108}$. Specifically, four of four selenium sites were located and used for SAD phasing, using phenix.hyss. Subsequently, Phaser (31) was used to calculate the experimental phases, followed by density modification with RESOLVE (32) (figure of merit 0.34 before and 0.65 after density modification). The experimental density map showed clear features of the protein backbone and well defined side chains. RESOLVE traced and automatically built 120 residues and their side chains in the experimental electron density. COOT (33) was used to manually correct the incorrectly modeled residues, and through successive iterative rounds of refinement and manual model building, the remaining residues were traced in the electron density to afford the final model. Restrained individual atomic refinement and restrained isotropic individual B-factor refinement with maximum likelihood targets using the Babinet model for bulk solvent scaling was performed using REFMAC5 (34) of the CCP4 suite (35). The final SeMet-CblD$^{\Delta N108}$ model, after the removal of residues with high B-factors and water molecules was used as a starting model for the refinement of CblD$^{\Delta N108}$ to 1.9 Å resolution. Initial simulated annealing refinement (torsional and Cartesian) was performed with phenix.refine followed by iterative rounds of refinement and model building/correcting with Refmac5 and Coot as described above. In the final CblD$^{\Delta N108}$ model, residues 109–117, and 123–131 are missing in one monomer and residues 108–132, 169, and 170 in the second monomer in the asymmetric unit. The missing residues were not modeled because no visible electron density associated with these residues was found. The geometric quality of the models was assessed with MolProbity (36). PyMOL (37) was used to create molecular images.

Results

Construct Design—Attempts to crystallize full-length CblD failed despite considerable effort. We therefore analyzed the primary sequence by DisEMBL (38), PrDOS (39), and PSIPRED (40) to detect possible disordered regions at the protein termini. All three servers predicted that CblD is highly disordered and lacks any secondary structure at the N-terminal region spanning approximately the first 100 amino acids. Therefore, we designed a variant in which the first 108 residues of human CblD were deleted, which we refer to as CblD$^{\Delta N108}$ (Fig. 1*B*).

Structure Determination—SAD phasing using the SeMet derivative was used to determine the crystal structure of CblD$^{\Delta N108}$ (Table 1). Phenix Autosol was used to calculate the initial phases, and the initial experimental maps were obtained at 2.31 Å resolution. A complete model was built and refined for the SeMet derivative that was subsequently used for obtaining a solution for the wild-type CblD$^{\Delta N108}$ structure to 1.9 Å resolution (Table 1). Because the structures of the wild-type and the SeMet derivative of CblD$^{\Delta N108}$ were identical, the higher resolution wild-type structure is discussed in the remainder of the text. In the wild-type structure, we find two molecules of CblD$^{\Delta N108}$ in the asymmetric unit, which is involved in dimer formation as discussed below. In the final refined model, we see clear and unambiguous electron density in both monomers for residues corresponding to the C-terminal region that spans from residues 132 to 296. The N-terminal region (residues 108–131), with the exception of a very short polypeptide (118–122) in one of the molecules in the asymmetric unit, was not modeled because no visible electron density corresponding to this region could be discerned. Therefore, the N-terminal region even in the truncated CblD$^{\Delta N108}$ variant is unstructured and disordered.

Overall Fold and Structure Description—The CblD$^{\Delta N108}$ structure exhibits a single domain of 152 residues (145–296) with an overall topologic arrangement characteristic of an $\alpha+\beta$ fold (Fig. 2). Specifically, the core of CblD$^{\Delta N108}$ is comprised of a central four-stranded anti-parallel β-sheet sandwiched between four α helices and a β hairpin. The anti-parallel β-sheet is enclosed on one side by a very long (αC) and a short (αE) helix (Fig. 2*A*, *left panel*) and on the other side by two short helices (αB and αD) and a β hairpin ($\beta1'$-$\beta2'$) that are arranged perpendicular to the central β-sheet (Fig. 2*A*, *right panel*). The loops that connect the various secondary structure elements comprising the core of CblD$^{\Delta N108}$ are numbered sequentially (Fig. 2*B*). This structural arrangement is comparable to that found in members of the NFR superfamily, which is discussed in detail later.

Dimer/Subunit Interaction—Although full-length CblD is reported to be a monomer in solution (22, 23), CblD$^{\Delta N108}$ is found as a dimer in the asymmetric unit (Fig. 3, *A* and *B*). Despite its extended interdomain interface (1435 Å^2 buried surface) containing multiple ionic and hydrophobic interac-

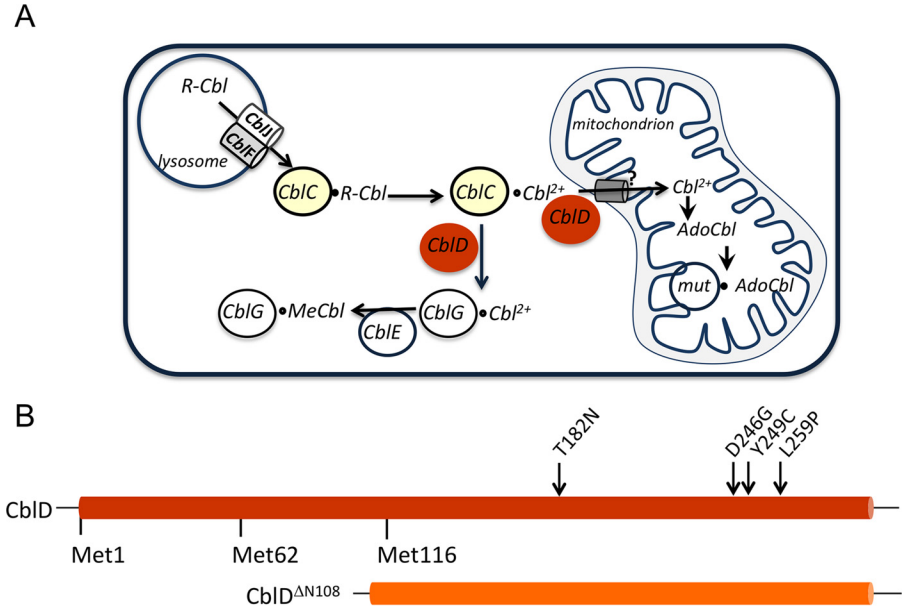

FIGURE 1. **The cobalamin trafficking pathway and boundaries of the CblD$^{\Delta N108}$ construct used in this study.** *A*, cobalamin first enters the lysosome from circulation, and CblC binds alkylcobalamin (*R-Cbl*) as it enters the cytoplasm via the action of two lysosomal membrane proteins. Following processing of cobalamin to a common cob(II)alamin (Cbl^{2+}) intermediate, it is partitioned into the cytoplasmic and mitochondrial pathways for cofactor assimilation. Although the precise function of CblD is unknown, it functions downstream of CblC. CblE (methionine synthase reductase) provides reducing equivalents needed for the conversion of cob(II)alamin to methylcobalamin (*MeCbl*), the active cofactor form for CblG (methionine synthase). MS^{act} binds AdoMet and provides the methyl group needed for MeCbl synthesis. For clarity, details of the mitochondrial pathway, where cob(II)alamin is converted to adenosylcobalamin (AdoCbl) and loaded into methylmalonyl-CoA mutase (*mut*) are not shown. The mechanism by which cobalamin enters the mitochondrion and the role of CblD in this process (denoted by a *question mark*) are unknown. *B*, boundaries of full-length CblD showing the N-terminal initiation site (Met^1) as well as two internal initiation sites (Met^{62} and Met^{116}). The locations of the missense patient mutations in CblD that result in isolated homocystinuria are indicated. The boundaries of the CblD^{N108} construct used for crystallography are shown below.

TABLE 1

X-ray crystallography data collection and refinement statistics

Parameter	CblD$^{\Delta N108}$	SeMet CblD$^{\Delta N108}$
Data collection		
Beamline	APS, GMCA 23-IDB	APS, GMCA 23-IDB
Wavelength (Å)	0.979	
Resolution (Å)	50.0–1.90 (1.97–1.90)	50.0–2.31 (2.39–2.31)
Space group	$P2_1$	I222
Cell dimensions (Å)	$a = 47.6, b = 67.1, c = 66.2$	$a = 65.3, b = 66.2, c = 71.8$
Cell dimensions (°)	$\alpha = 90, \beta = 110.5, \gamma = 90$	$\alpha = \beta = \gamma = 90$
Unique reflections	30,281 (2986)	6667 (488)
Multiplicity	3.2 (2.8)	7.0 (3.5)
Completeness (%)	98.1 (97.0)	94.1 (70.4)
$<I/\sigma>$	13.1 (2.5)	14.5 (2.5)
R_{merge} (%)	7.9 (41.7)	9.8 (35.9)
Refinement		
Resolution range	62.01–1.90	48.71–2.31
Number of reflections (work/test set)	28,735/1523	6338/320
Number of atoms (protein/water)	2666/303	1266/21
Mean B-factors Å^2	26.2/33.6	45.2/36.7
R_{work}/R_{free} (%)	18.8/22.7	20.8/26.3
Root mean square deviation from ideal values (bonds, Å)	0.12	0.11
Root mean square deviation from ideal values (angles, °)	1.39	1.37
Ramachandran plot (favored/outliers, %)	99.4/0.0	96.1/0.0
MolProbity Score	1.01 (100th percentile)	1.75 (97th percentile)
Protein Data Bank code	5CV0	5CUZ

tions, the dimer is most likely a crystallization artifact. The N-terminal region (referred to as the "dimerization arm"), comprising a small helix αA and two loops (L1 and L2) spanning residues 132–145, promotes dimerization and contributes mostly to the dimer interface. The dimer interface is assembled mostly via two types of contributions, an "arm and arm" and an "arm and body." In the "arm and arm" type of interaction, one dimerization arm and specifically the L2 region, interacts with the corresponding region (L2′) in the adjacent monomer (Fig. 3*B*). This "arm and arm" part of the interface is mostly electrostatic in nature and involves interactions detailed in Fig. 3*C*. In the "arm and body" interface, one dimerization arm and specifically the L1 region and helix αA of one monomer make contact with helices αC and αE and strand β1 in the adjacent monomer. In the crevice formed between the subunits at the "arm and body" interface, a combination of mainly hydrophobic and a few electrostatic interactions are involved (Fig. 3*D*).

Because both the full-length and the variously truncated forms of CblD reportedly behave as monomers in solution (22, 23), we used ultracentrifugation analysis to investigate the olig-

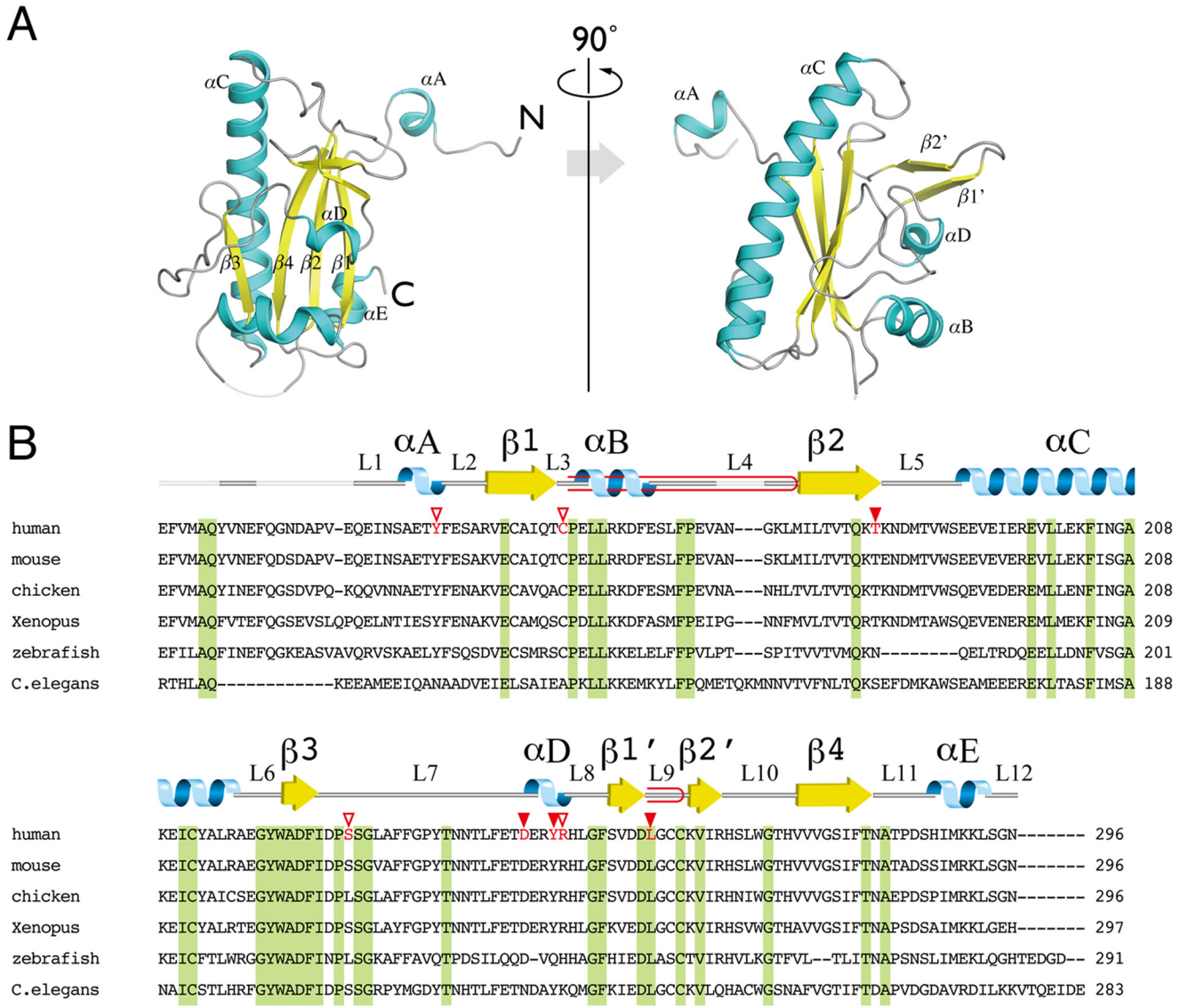

FIGURE 2. **Structure of CblD$^{\Delta N108}$ and location of patient mutations.** *A*, the structure of CblD$^{\Delta N108}$ is illustrated in ribbon diagram, with α helices and β sheets colored *cyan* and *yellow*, respectively. *B*, the secondary structure of CblD$^{\Delta N108}$ is illustrated above the sequence alignments of CblD from different organisms. The α helices and β sheets are shown in *cyan* and *yellow*, respectively. The amino acid alignment is of CblDs from human (GenBank™ accession number, NP_056517), mouse (NP_598600), chicken (NP_001008477), *Xenopus* (NP_001089489), zebrafish (NP_001002453), and *Caenorhabditis elegans* (NP_499801). Residues that are conserved across the species are highlighted in *green*. Residues shown in *red letters* correspond to *cblD* patient mutations with the *filled* and *open arrowheads* above them representing missense and nonsense mutations, respectively. *Red loops* indicate β-hairpins. The secondary structure representation was generated with PDBsum, and the multiple sequence alignment was generated with Clustal Omega (1.2.0).

omeric state of CblD$^{\Delta N108}$. Based on this analysis, CblD$^{\Delta N108}$ also behaves as a monomer in solution even at concentrations (10 mg/ml) that were used for crystallization (data not shown). Thus, the unique dimerization mode of CblD$^{\Delta N108}$ as observed *in crystallo* is clearly distinct from the dimerization mode of the CblD structural homologs that belong to the NFR family members and will be detailed later.

Identification of CblD Structural Homologs—Prior to this study, the *cblD* gene product was listed as an "uncharacterized conserved protein (DUF2246)" in the NCBI conserved domain database with no available structural homolog. Our initial DALI search (41) revealed that the closest structural homologs of CblD$^{\Delta N108}$ are CblC, some members of the NFR superfamily (Conserved Domain Database accession number cl00514), *e.g.* BluB from *Sinorhizobium meliloti* and flavin reductase P from *Vibrio harveyi*, and MS^{act}, the activation domain of cobalamin-dependent MS. These proteins exhibit high structural similarity (z score >4) despite their very low sequence similarity (3–18% identity). In addition to these proteins, two corrinoid-dependent dehalogenases (26, 27) that are topologically similar to CblC (28) have been described recently.

CblD, CblC, NpRhdA (a corrinoid-dependent reductive dehalogenase from *Nitratireductor pacificus* pht-3B), and MS^{act} share common structural features (within the *blue rectangle*), including a characteristic β-hairpin, which distinguishes them from other NFR family members (Fig. 4). In Fig. 4, the *red dotted boxes* represent the most conserved feature in all proteins described here including those belonging to a typical NFR family member, whereas the *blue boxes* include features exclusively shared by CblD, CblC, NpRhdA, and MS^{act}, but not

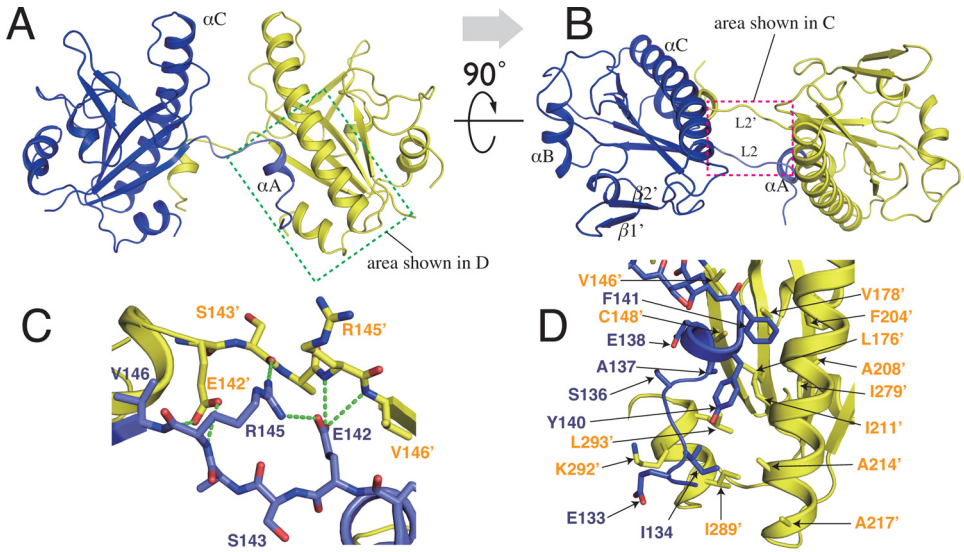

FIGURE 3. **Structure of the CblD$^{\Delta N108}$ homodimer.** *A* and *B*, two views of the CblD$^{\Delta N108}$ dimer shown in ribbon representation with the subunits colored in *blue* and *yellow*, respectively. The N-terminal region including the extended α helix (αA) and the L2 loop (up to residue Arg^{145}) is the primary contributor of the dimer interface. *C*, close-up of the arm to arm subunit interface (*pink dotted box* in *B*). Amino acid residues involved in the interface analyzed by PISA are shown in stick representation. Hydrogen bonds and salt bridges are found in the loop region (Glu^{142}–Arg^{145}, between αA and β1). Specifically salt bridges between Glu^{142} and Arg$^{145\prime}$, hydrogen bonds between the Glu^{142} side chain carboxylate and the Arg$^{145\prime}$ and Val$^{146\prime}$ backbone amido groups, the Glu$^{142\prime}$ side chain carboxylate and the Arg^{145} and Val^{146} backbone amido groups, and the Arg^{145} amine side chain with the Ser$^{143\prime}$ backbone carbonyl are highlighted. *D*, close-up of the arm to body interface (*green dotted box* in *A*). Specifically, the hydrophobic interface is lined up by residues Ile^{134}, Ser^{136}, Ala^{137}, Tyr^{140}, and Phe^{141} in the arm of one monomer and the residues Val$^{146\prime}$, Cys$^{148\prime}$, Leu$^{176\prime}$, Val$^{178\prime}$, Phe$^{204\prime}$, Gly$^{207\prime}$, Ala$^{208\prime}$, Ile$^{211\prime}$, Ala$^{214\prime}$, Ala$^{217\prime}$, Ile$^{279\prime}$, Ile$^{289\prime}$, and Leu$^{293\prime}$ all found in a crevice formed from helices αC and αE and strand β1 of the adjacent monomer. The electrostatic interactions in the arm and body part are formed through hydrogen bonds between the Ala^{137} backbone amide and Leu$^{293\prime}$ carbonyl, the Glu^{138} side chain carboxylate and the Cys$^{148\prime}$ backbone amide, and a salt bridge between Glu$^{133\prime}$ and Lys^{292}. In *C* and *D*, hydrogen bonds and salt bridges are shown by *dotted green lines*.

by other proteins in the NFR superfamily. These conserved structural features are relevant to the cobalamin-related biological functions of these proteins as discussed later.

CblD Is Similar but Different from Other NFR Family Members—A detailed comparison of CblD was made with the NFR family member, *BluB* (Fig. 5*A*). Superposition of CblD$^{\Delta N108}$ and BluB monomers (Fig. 5*B*) with Swiss-Pdb Viewer gives a root mean square deviation of 1.33 Å based on 53 of 152 structurally equivalent residues, 22% identity). The central anti-parallel β-sheet bundle is found in nearly identical positions in both proteins, whereas the arrangement of the surrounding α-helices is very similar. Of particular note is the near ideal superposition of a long α-helix (αC in CblD$^{\Delta N108}$ (Fig. 2*A*) and αE in BluB (Fig. 5*A*), which is a structural hallmark of the NFR family. The majority of NFR family members exist as homodimers, and the long α-helix is important for dimerization. The flavin- and substrate-binding sites are located at the dimer interface in these proteins. In contrast, CblD and CblC do not form dimers in solution, and the dimerization interface seen in their crystal structures is distinct from that of other NFR family members in that it does not involve the long helix (28, 42).

Substantially more contact area (≈4800 Å^2) is buried at the interface of the BluB dimer (Fig. 5*C*) than the CblD$^{\Delta N108}$ dimer (≈1435 Å^2). By superimposing two molecules of CblD$^{\Delta N108}$ on a BluB dimer, a theoretical homodimerization model for CblD$^{\Delta N108}$ was generated (Fig. 5*D*). The αC helices from both CblD$^{\Delta N108}$ monomers in *dark blue* and *yellow* can theoretically align and assemble an interface similar to that in BluB. However, other interactions at the interface that are present in BluB and other NFR family members are missing in CblD$^{\Delta N108}$. These include the long N-terminal region including helix αA and the β-strand (β5) in BluB that are important in the dimer interface (Fig. 5*C*). Based on this analysis, we conclude that neither CblD nor CblC has the capacity to dimerize in the same mode as other members of the NFR superfamily, despite sharing a similar core subunit topology (Fig. 4).

CblC Is the Closest Structural Homolog of CblD—Although CblC and CblD share little sequence similarity, their overall topology is remarkably similar with a root mean square deviation value of 1.5 Å based on 70 Cα atoms (Fig. 6, *A* and *B*). Solution of the crystal structure of CblC led to the recognition that it resembles some members in the NFR superfamily (28, 42). CblC and CblD share an identical core of antiparallel β-sheets with similar structural elements in comparable arrangements framing the core. Both proteins exhibit superimposable long helices (αC in CblD and αE in CblC), and the arrangements of the structural components between strands β3 and β4 are very similar. Specifically, following strand β3, a long loop (*L*7 in CblD spanning residues 226–245 and *L*9 in CblC spanning residues 103–116) is present, followed by a short helix (αD in CblD and αF in CblC). Furthermore, a β-hairpin (β1′ and β2′) and a loop connecting to strand β4 (*L*10 in CblD (residues: 267–274), and *L*13 in CblC (residues: 151–158)) are found in perfectly superimposable positions in both proteins. Although the residues spanning the β1 and β2 strands adopt different conformations in the two proteins, they are nonetheless found in approximately similar locations.

Despite the similarities between the two proteins, there are also a number of differences. CblC has a four-helical cap comprising αI-αL (Fig. 6*A*) that is situated on top of the core domain and is absent in CblD. The long αE helix that facilitates

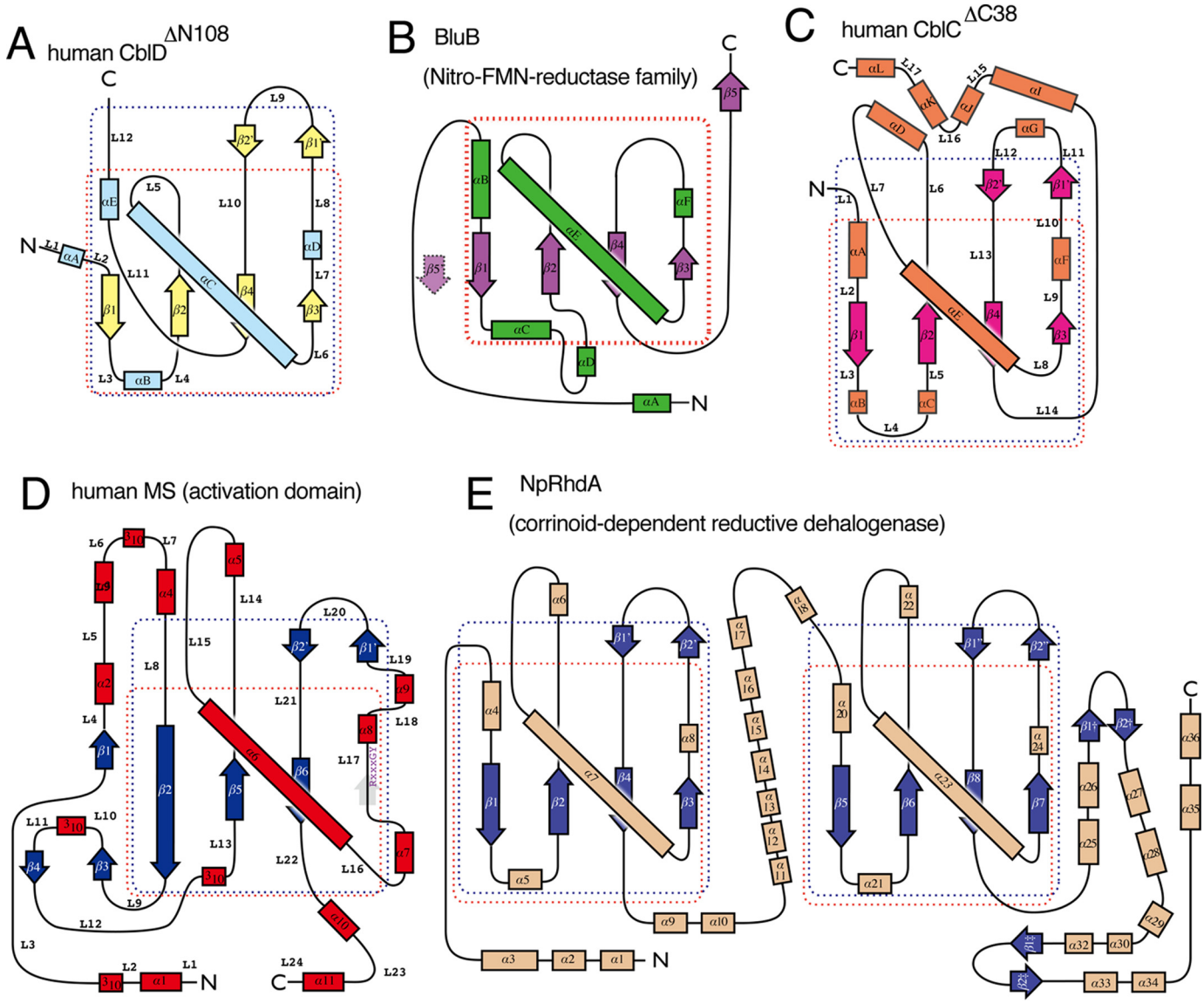

FIGURE 4. **Topological comparison within the structural neighborhood of CblD.** Diagrams of the secondary structures of CblD$^{\Delta N108}$ (*A*), BluB (*B*) (48), CblC (*C*) (28), human MS^{act} (*D*) (44), and NpRhdA (*E*) (26) are shown. The numbering and assignments of the secondary structures are from Ref. 48. In *B*, the extra β sheet (outside the *dotted box*) is from the second subunit of BluB, which is a homodimer. In *D*, the numbering and naming of the secondary structure elements are from Ref. 44, except for β1′, β2′, and β6, which were originally described as β6, β7, and β8, respectively. PDBsum was used to analyze the topology of NpRhd.

dimerization in other members of the NFR family is not continuous in CblC and therefore shorter than the corresponding helix in CblD (Fig. 6*B*). We had previously suggested that the presence of the four-helical cap in CblC forces what could be a continuous helix, such as αC in CblD, to bend and break into two helices αE and αF (28). Another difference is that the loop following strand β3 (*L7* and *L9* in CblD and CblC, respectively), is six amino acids longer in CblD. In CblC, this loop adopts two distinct conformations depending on the presence or absence of cobalamin. The binding of cobalamin induces a conformational change that allows loop *L9* to move closer to the four-helical cap and to contribute to the cobalamin-binding pocket. Loop *L7* in CblD adopts a conformation similar to that of loop *L9* in CblC in the absence of cobalamin. Furthermore, the loop between the two β-strands in the β-hairpin, is approximately three times shorter in CblD. Finally, a functionally significant difference between the two proteins is the presence of a large cavity in CblC that accommodates cobalamin but is largely occluded in CblD (Fig. 6*C*). Indeed, attempts to dock cobalamin in the CblD cavity were largely unsuccessful. In addition, the four-helical cap forms part of the cobalamin-binding pocket in CblC and, as noted, is missing in CblD. Instead, the long αC helix and the loop connecting to β3 occupy a region in CblD corresponding to the cobalamin-binding pocket in CblC. These large structural protrusions along with smaller ones would lead to steric clashes with cobalamin, explaining the observed lack of binding of this cofactor to CblD (22, 23).

Topological Similarities between CblD, MS^{act}, and Corrin-dependent Reductive Dehalogenases—Cobalamin-dependent methionine synthase is a multidomain protein in which the terminal module constitutes the activation domain (Fig. 7*A*). MS^{act} binds *S*-adenosylmethionine (AdoMet) and is important

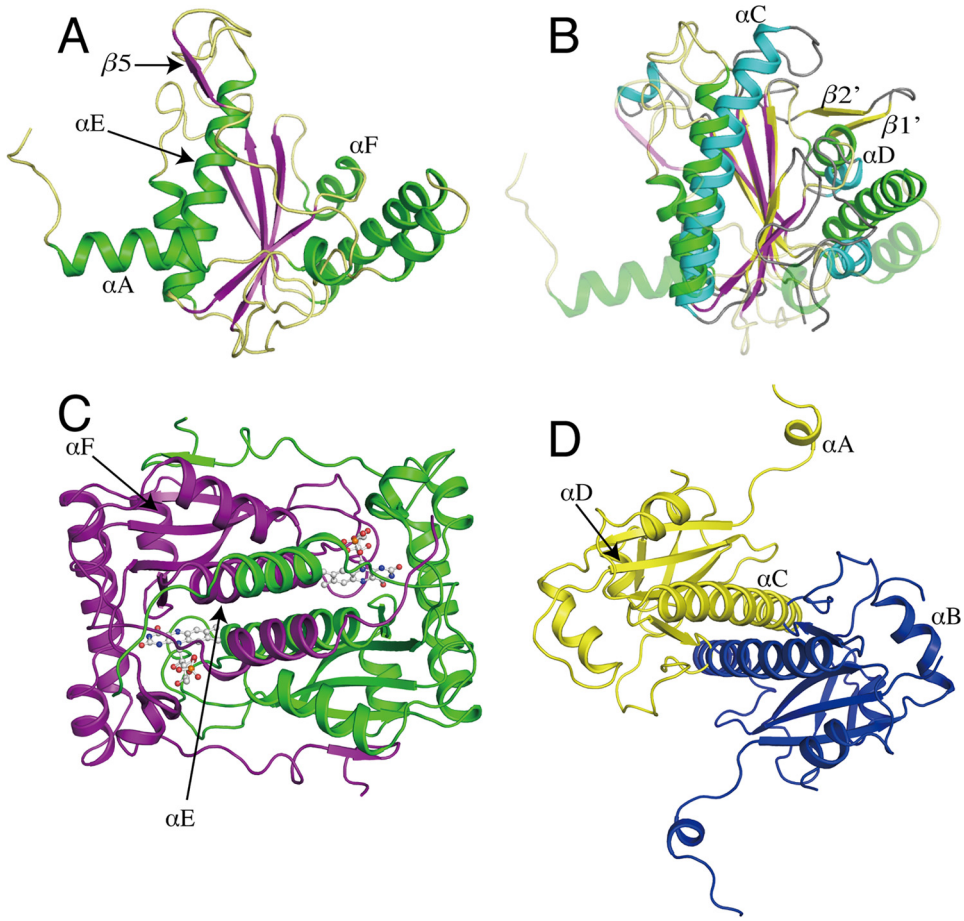

FIGURE 5. **Structural comparison between CblD and BluB.** *A*, the BluB monomer is shown in ribbon representation with α helices and β sheets shown in *green* and *purple*, respectively. *B*, superposition of BluB and CblD$^{\Delta N108}$ monomers. *C*, organization of the BluB dimer (Protein Data Bank code 2ISJ) is distinct from that of CblD (Fig. 3*A*). The BluB monomers are shown in *green* and *purple*, respectively, and FMN is shown in ball and stick representation. *D*, modeled homodimer of CblD$^{\Delta N108}$ constructed by superimposing two monomers onto a BluB dimer as described under "Results." The CblD$^{\Delta N108}$ subunits are in *blue* and *yellow*.

for repairing inactive cobalamin bound in the preceding domain (43, 44). Human MS^{act} is approximately twice the size of CblD$^{\Delta N108}$ and therefore exhibits additional features. Nevertheless, topological similarities are evident between them in their core regions (Fig. 7*B*).

The crystal structures of two corrinoid-dependent reductive dehalogenases, NpRdhA (26) and PceA (27), were recently reported. Both enzymes harbor two iron/sulfur clusters and bind one corrinoid cofactor per monomer. NpRhdA shown in Fig. 7*C* is a monomer and binds the corrin cofactor at the C terminus, whereas PceA is a homodimer. The corrinoid-binding domains in NpRhdA and PceA are similar to that of CblC and distinct from the classic Rossmann fold-containing motif found in other cobalamin proteins (45, 46). The CblD structure superimposes very well on the corrin-binding domains of NpRhdA (Fig. 7*D*) and PceA (data not shown). It is interesting that although CblD does not bind a corrin cofactor, its topology is more similar to that of CblC and the reductive dehalogenases than to other member of the NFR superfamily. We propose that these proteins (CblC, CblD, PceA, and NpRdhA) constitute a new subfamily within the NFR superfamily and are distantly related to the other NFR family members.

Putative Ligand Binding Sites in CblD—Because CblD does not bind cobalamin, we looked for similarities between CblD and the MS^{act} domain. Like CblD, MS^{act} does not bind cobalamin but binds AdoMet in a pocket (indicated by an *arrow* in Fig. 7*A*). The equivalent location in CblD is partially occupied by loop L7 and is thus unlikely to serve as a pocket for binding AdoMet. Interestingly, this equivalent location in CblD corresponds to a putative flavin-binding site in CblC that forms only when cobalamin is not bound (28). When cobalamin binds, structural changes to L9 (equivalent to L7 in CblD) open up the putative flavin-binding pocket. It is thus conceivable that conformational changes occur when CblD interacts with a physiological partner leading to reorganization in the region of the L7 loop and creating a ligand-binding cavity. Nonetheless, CblD alone is unable to bind ATP, GTP, AdoMet, NADP$^+$, or NADPH (data not shown).

Location of Pathogenic Missense Mutations and Their Effects on CblD Function—The majority of the disease-causing mutations in CblD result in either frameshifts or premature termination (11), leading to an expected loss of function. The four known missense disease-causing mutations can now be mapped on the CblD structure (Fig. 8*A*). Three of the four mutations cluster at one surface. D246G resides in loop 7, Y259C is in the αD helix, and L259P is in the β-hairpin. Interestingly, the position comparable to the αD helix and the β-hairpin in MS^{act} is proximal to the AdoMet-binding site or to

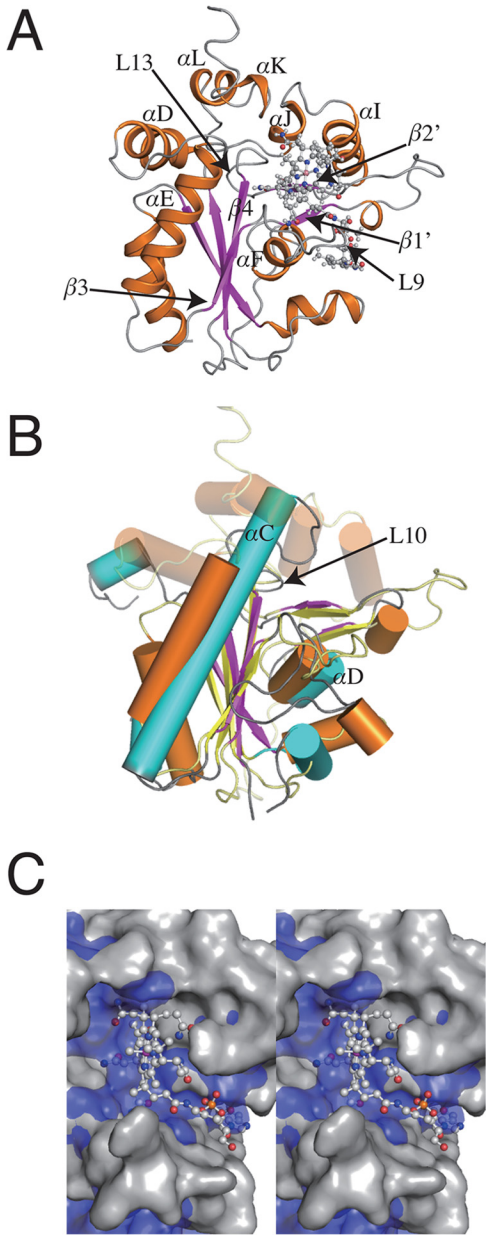

FIGURE 6. **Structural comparison between CblD and CblC.** *A*, the structure of CblC$^{\Delta C38}$ (Protein Data Bank code 3SC0) is shown with α helices and β sheets in *orange* and *magenta*, respectively, and cobalamin is in ball and stick representation. *B*, superposition of CblC and CblD in which the helices are shown as *cylinders*. *C*, close-up of the superposition of CblD (*blue*) and the cobalamin-binding site of CblC (*gray*) displayed in a space-filling representation and shown in stereo view. Methylcobalamin bound to CblC is shown in ball and stick representation. The CblC B_{12}-binding site is overlaid onto the equivalent region in CblD so as to show that CblD residues (*blue*) project into the B_{12} binding cavity in CblC (*gray*) and, as a result, preclude B_{12} binding.

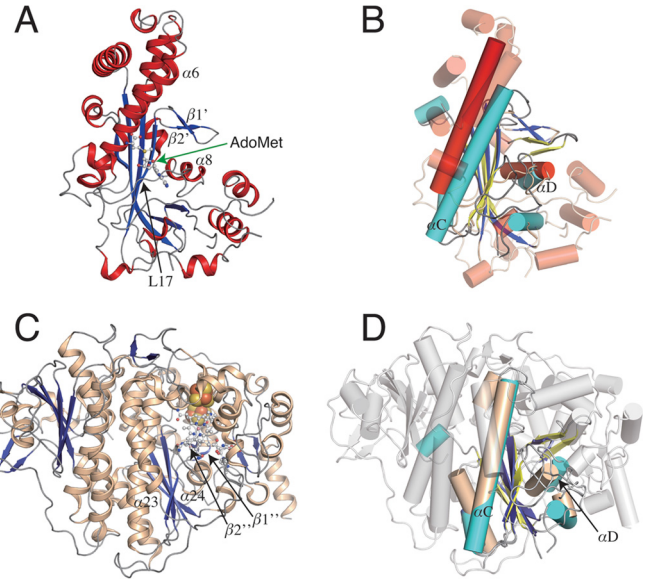

FIGURE 7. **A structural comparison between CblD$^{\Delta N108}$, MS^{act}, and NpRhdA.** *A*, structure of human MS^{act} (Protein Data Bank code 2O2K) with α helices and β sheets colored *red* and *blue*, respectively, and AdoMet (indicated by the *green arrow*) is shown in ball and stick representation. *B*, superposition of the structures of CblD$^{\Delta N108}$ and MS^{act}. *C*, structure of NpRhdA is shown in ribbon diagram (Protein Data Bank code 4RAS) in which cobalamin and the iron-sulfur clusters are shown in ball and stick mode and sphere representation, respectively. *D*, superposition of the B_{12}-binding domain of NpRhdA and CblD. The extra elements in NpRhdA are displayed in *light gray*.

the site that interacts with the cobalamin-binding domain in methionine synthase (47). The fourth mutation, T182N, is located at the end of the β2 strand (Fig. 2*B*).

We have previously reported that CblD interacts with CblC albeit only when the product of the CblC reaction, cob(II)alamin, is bound to CblC (23). When reconstituted with cob(II)alamin, CblC protects it from further oxidation to OH_2Cbl (Fig. 8*C*, $v = 0.067 \pm 0.009$ nmol h^{-1}). Surprisingly, in the presence of stoichiometric CblD, the kinetics of cob(II)alamin oxidation is significantly enhanced ($v = 1.81 \pm 0.09$ nmol h^{-1})). All four pathogenic mutations diminish the rate of CblC-bound cob(II)alamin oxidation (T182N CblD, $v = 1.33 \pm 0.19$ nmol h^{-1}, D246G CblD: $v = 1.24 \pm 0.10$ nmol h^{-1}, Y249C CblD: $v = 0.57 \pm 0.09$ nmol h^{-1}, and L259P CblD: $v = 0.47 \pm 0.05$ nmol h^{-1}).

A phage display study was previously employed to identify putative peptides on CblD that might be important for its interactions with CblC. As shown in Fig. 8*D*, these peptides are diffusely scattered across the surface of CblD and therefore are of limited utility in delineating the CblD surface that interacts with CblC.

Discussion

Herein, we report the first structure of human CblD, a protein involved in intracellular cobalamin trafficking. Based on the clinical phenotypes of patients with the *cblD* disorder, the protein is predicted to play an important role in intercellular cobalamin delivery to both the cytosolic and mitochondrial targets, methionine synthase and methylmalonyl-CoA mutase (17). However, despite identification of the gene associated with the *cblD* locus in 2008 (11), insights into its function have been limited primarily because of its lack of sequence similarity to other proteins and its inability to bind cobalamin or other ligands that have been tested.

The *cblD* gene encodes a protein (from the Met^1 initiation codon; Fig. 1*B*)) with a weak mitochondrial leader sequence at the N terminus, consistent with its proposed role in the mitochondrial branch of cobalamin metabolism (11). Replacement of the CblD leader sequence with a more efficient one from aldehyde dehydrogenase 2 improved adenosylcobalamin synthesis and cobalamin delivery to methylmalonyl-CoA mutase

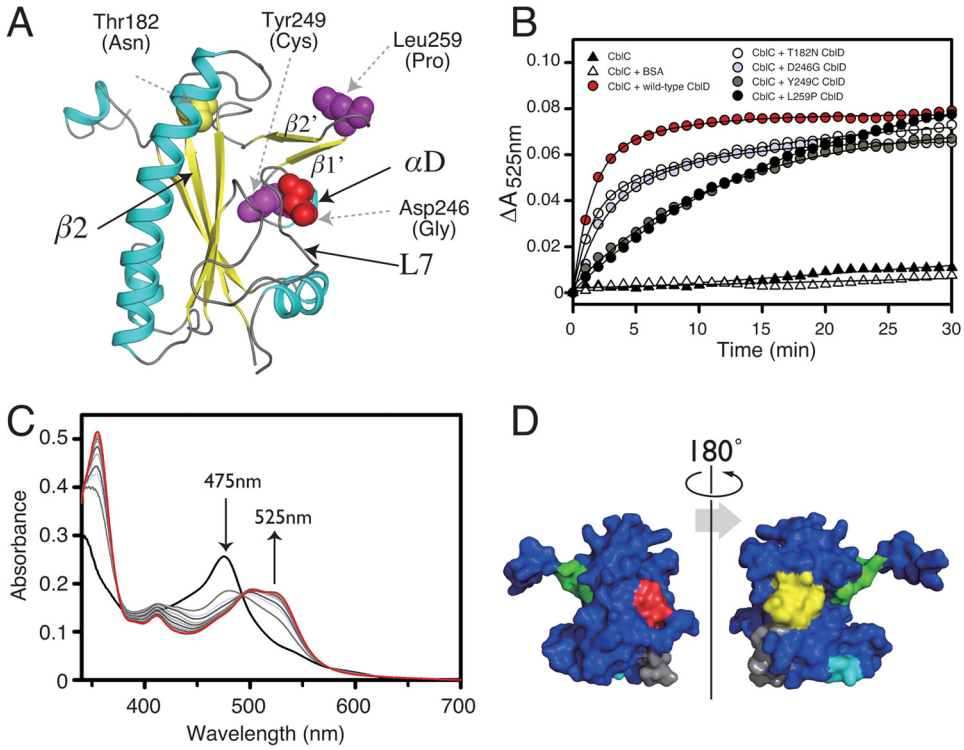

FIGURE 8. **Locations of CblD missense mutations and their biochemical effects.** *A*, the structure of CblD$^{\Delta N108}$ indicating the positions of the disease-causing missense mutations: Thr^{182} (*yellow*), Asp^{246} (*red*), Tyr^{249} (*magenta*), and Leu^{259} (*purple*). The pathogenic amino acid substitutions are in *parentheses*. *B*, time-dependent changes in the UV-visible absorption spectra of cob(II)alamin (30 μM) bound to CblC (30 μM) in 100 mM HEPES, pH 7.4, 150 mM KCl, and 10% (v/v) glycerol following oxidation in the presence of CblD$^{\Delta N115}$ (30 μM). *Black trace*, 0 min, λ_{max} = 475 nm; *red trace*, 30 min, λ_{max} = 525 nm; *gray traces*, intermediate time points. *C*, kinetics of the oxidation of cob(II)alamin (30 μM) bound to CblC (30 μM) in the absence or the presence of 30 μM wild-type or mutant CblD as indicated. In a control reaction, the oxidation of cob(II)alamin was also monitored in the presence of 1 mg/ml of BSA. The reactions were initiated by the addition of an anaerobic CblC-cob(II)alamin mixture to an aerobic solution containing BSA or CblD as described under "Experimental Procedures." *D*, location of CblD peptides identified by phage display and postulated to be important for interaction with CblC. The displayed peptides are shown in *green* (residues 143–147), *gray* (residues 157–168), *red* (residues 226–232), *yellow* (residues 250–256), and *cyan* (residues 281–288).

(25). Patients carrying nonsense mutations at the 5′-end of the gene express N-terminally truncated CblD variants that are presumably translated by use of internal initiation sites, presumably Met^{62} or Met^{116} (Fig. 1*B*). These truncated variants can support cobalamin-dependent methionine synthase function (25). Based on these observations, it has been proposed that CblD functions in directing cobalamin delivery, with the N- and C-terminal portions of the protein being important for supporting methylmalonyl-CoA mutase and methionine synthase functions, respectively (11, 25). The CblD$^{\Delta N108}$ variant used in this study includes the internal Met^{116} initiation site and the residues where mutations have been reported in *cbl*D patients exhibiting isolated methylmalonic acidura or combined homocystinuria and methylmalonic aciduria. Hence, whereas the truncated protein used in our study lacks a large N-terminal segment that is presumed to be disordered, it is nevertheless relevant for understanding how CblD functions in the cytoplasmic branch of the cobalamin trafficking pathway.

The most striking feature of the ordered C-terminal half of CblD (residues 145–296) is that it exhibits a structural fold very similar to that found in CblC, which was not expected. We speculate that this architectural similarity despite the lack of sequence similarity could be functionally important for CblD, which is predicted to operate immediately downstream of CblC in the trafficking pathway (Fig. 1). The molecular mimicry might be functionally important if CblC and CblD compete for binding to the same surface on a target protein in the trafficking pathway. It is possible that CblC and CblD arose via a distant gene duplication event followed by loss of the cofactor-binding site, which led to the functional speciation of CblD.

We know that CblD forms a stable complex with CblC albeit only under conditions where the product of the CblC processing reaction, cob(II)alamin, is bound (23). In this study, we demonstrate that the CblC-bound cob(II)alamin becomes more prone to oxidation in the presence of CblD forming OH_2Cbl, presumably by increasing access of oxygen to the cobalt ion in CblC (Fig. 8, *B* and *C*). The significance of this observation is presently not known and is being investigated. However, this initial observation is noteworthy on two accounts. First, because CblC displays a lower affinity for OH_2Cbl than for cob(II)alamin, enhanced oxidation in the CblC-CblD complex might be important for its subsequent transfer to a donor protein. Second, all four pathogenic mutations reduce the rate of CblC-bound cob(II)alamin oxidation. These observations are consistent with the initially proposed adaptor function of CblD (4). The folded and globular C-terminal region is sufficient for complex formation with CblC (23) and for supporting the cytoplasmic branch of the trafficking pathway. In contrast, an additional and seemingly unstructured N-terminal region is needed for the mitochondrial branch of the trafficking pathway and presumably becomes ordered in complex with a partner protein.

Two of the members of the new NFR subfamily that we have described here (CblD and MS^{act}) do not bind cobalamin directly but interact with proteins (CblC) or domains (B_{12} domain of methionine synthase) that do. The structure of the C-terminal half of methionine synthase comprising the cobalamin- and MS^{act} domains (47) shows that the MS^{act} module interacts via a unique β-hairpin ($\beta1'$-$\beta2'$) with a propionamide side chain of cobalamin in the adjacent B_{12}-binding module. The corresponding β-hairpin element is found in identical positions in CblD, CblC and in the reductive dehalogenases. Interestingly, in the B_{12}-binding proteins, *i.e.* CblC and the reductive dehalogenases, the β-hairpin structure is directly involved in cofactor binding. In CblC, the corrin ring stacks against the hairpin, which also contributes to the wall of the groove into which the dimethylbenzimidazole moiety of cobalamin binds (28). We posit that the β-hairpin structure in CblD competes with the equivalent structure in CblC in a protein-protein complex and interacts with the cobalamin. Interestingly, three of the disease-causing missense mutations are located in the vicinity of the β-hairpin (Fig. 8*A*).

In summary, although the precise role of CblD remains elusive, the structure of its globular C-terminal domain reveals a surprising and unexpected structural similarity to CblC, with which this domain interacts. Together with the newly described structures of other corrinoid proteins that do not use the canonical Rossmann fold for binding B_{12}, they have allowed delineation of a new subfamily within the NFR superfamily that share unique structural features. Finally, the CblD structure allows mapping of disease-causing mutations identified in patients with the *cblD* disorder.

Author Contributions—K. Y., C. G., R. B., and M. K wrote the manuscript. C. G. expressed and purified the protein and performed biochemical analysis. K. Y. crystallized the protein, and K. Y. and M. K. collected crystallographic data, solved the structure, and performed structural analysis. All authors edited and approved the final version of the manuscript.

Acknowledgments—We acknowledge GM/CA CAT at the Advanced Light Source for beam time. We thank Deepa Rajagopalan for help with the construction of CblD mutants.

References

1. Mellman, I. S., Youngdahl-Turner, P., Willard, H. F., and Rosenberg, L. E. (1977) Intracellular binding of radioactive hydroxocobalamin to cobalamin-dependent apoenzyme in rat liver. *Proc. Natl. Acad. Sci. U.S.A.* **74,** 916–920
2. Kolhouse, J. F., and Allen, R. H. (1977) Recognition of two intracellular cobalamin binding proteins and their recognition as methylmalonyl-CoA mutase and methionine synthetase. *Proc. Natl. Acad. Sci. U.S.A.* **74,** 921–925
3. Gherasim, C., Lofgren, M., and Banerjee, R. (2013) Navigating the B_{12} road: assimilation, delivery and disorders of cobalamin. *J. Biol. Chem.* **288,** 13186–13193
4. Banerjee, R., Gherasim, C., and Padovani, D. (2009) The tinker, tailor, soldier in intracellular B_{12} Trafficking. *Curr. Opin. Chem. Biol.* **13,** 484–491
5. Banerjee, R. (2006) B_{12} trafficking in mammals: A case for coenzyme escort service. *ACS Chem. Biol.* **1,** 149–159
6. Stabler, S. P. (2013) Clinical practice. Vitamin B_{12} deficiency. *N. Engl. J. Med.* **368,** 149–160
7. Gulati, S., Baker, P., Li, Y. N., Fowler, B., Kruger, W., Brody, L. C., and Banerjee, R. (1996) Defects in human methionine synthase in cblG patients. *Hum. Mol. Genet.* **5,** 1859–1865
8. Leclerc, D., Campeau, E., Goyette, P., Adjalla, C. E., Christensen, B., Ross, M., Eydoux, P., Rosenblatt, D. S., Rozen, R., and Gravel, R. A. (1996) Human methionine synthase: cDNA cloning and identification of mutations in patients of the *cblG* complementation group of folate/cobalamin disorders. *Hum. Mol. Genet.* **5,** 1867–1874
9. Lerner-Ellis, J. P., Tirone, J. C., Pawelek, P. D., Doré, C., Atkinson, J. L., Watkins, D., Morel, C. F., Fujiwara, T. M., Moras, E., Hosack, A. R., Dunbar, G. V., Antonicka, H., Forgetta, V., Dobson, C. M., Leclerc, D., Gravel, R. A., Shoubridge, E. A., Coulton, J. W., Lepage, P., Rommens, J. M., Morgan, K., and Rosenblatt, D. S. (2006) Identification of the gene responsible for methylmalonic aciduria and homocystinuria, cblC type. *Nat. Genet.* **38,** 93–100
10. Rutsch, F., Gailus, S., Miousse, I. R., Suormala, T., Sagné, C., Toliat, M. R., Nürnberg, G., Wittkampf, T., Buers, I., Sharifi, A., Stucki, M., Becker, C., Baumgartner, M., Robenek, H., Marquardt, T., Höhne, W., Gasnier, B., Rosenblatt, D. S., Fowler, B., and Nürnberg, P. (2009) Identification of a putative lysosomal cobalamin exporter altered in the cblF defect of vitamin B_{12} metabolism. *Nat. Genet.* **41,** 234–239
11. Coelho, D., Suormala, T., Stucki, M., Lerner-Ellis, J. P., Rosenblatt, D. S., Newbold, R. F., Baumgartner, M. R., and Fowler, B. (2008) Gene identification for the cblD defect of vitamin B_{12} metabolism. *N. Engl. J. Med.* **358,** 1454–1464
12. Coelho, D., Kim, J. C., Miousse, I. R., Fung, S., du Moulin, M., Buers, I., Suormala, T., Burda, P., Frapolli, M., Stucki, M., Nürnberg, P., Thiele, H., Robenek, H., Höhne, W., Longo, N., Pasquali, M., Mengel, E., Watkins, D., Shoubridge, E. A., Majewski, J., Rosenblatt, D. S., Fowler, B., Rutsch, F., and Baumgartner, M. R. (2012) Mutations in ABCD4 cause a new inborn error of vitamin B_{12} metabolism. *Nat. Genet.* **44,** 1152–1155
13. Yu, H. C., Sloan, J. L., Scharer, G., Brebner, A., Quintana, A. M., Achilly, N. P., Manoli, I., Coughlin, C. R., 2nd, Geiger, E. A., Schneck, U., Watkins, D., Suormala, T., Van Hove, J. L., Fowler, B., Baumgartner, M. R., Rosenblatt, D. S., Venditti, C. P., and Shaikh, T. H. (2013) An X-linked cobalamin disorder caused by mutations in transcriptional coregulator HCFC1. *Am. J. Hum. Genet.* **93,** 506–514
14. Dobson, C. M., Wai, T., Leclerc, D., Kadir, H., Narang, M., Lerner-Ellis, J. P., Hudson, T. J., Rosenblatt, D. S., and Gravel, R. A. (2002) Identification of the gene responsible for the *cblB* complementation group of vitamin B_{12}-dependent methylmalonic aciduria. *Hum. Mol. Genet.* **11,** 3361–3369
15. Dobson, C. M., Wai, T., Leclerc, D., Wilson, A., Wu, X., Doré, C., Hudson, T., Rosenblatt, D. S., and Gravel, R. A. (2002) Identification of the gene responsible for the *cblA* complementation group of vitamin B_{12}-responsive methylmalonic acidemia based on analysis of prokaryotic gene arrangements. *Proc. Natl. Acad. Sci. U.S.A.* **99,** 15554–15559
16. Lerner-Ellis, J. P., Anastasio, N., Liu, J., Coelho, D., Suormala, T., Stucki, M., Loewy, A. D., Gurd, S., Grundberg, E., Morel, C. F., Watkins, D., Baumgartner, M. R., Pastinen, T., Rosenblatt, D. S., and Fowler, B. (2009) Spectrum of mutations in MMACHC, allelic expression, and evidence for genotype-phenotype correlations. *Hum. Mutat.* **30,** 1072–1081
17. Suormala, T., Baumgartner, M. R., Coelho, D., Zavadakova, P., Kozich, V., Koch, H. G., Berghaüser, M., Wraith, J. E., Burlina, A., Sewell, A., Herwig, J., and Fowler, B. (2004) The *cblD* defect causes either isolated or combined deficiency of methylcobalamin and adenosylcobalamin synthesis. *J. Biol. Chem.* **279,** 42742–42749
18. Mah, W., Deme, J. C., Watkins, D., Fung, S., Janer, A., Shoubridge, E. A., Rosenblatt, D. S., and Coulton, J. W. (2013) Subcellular location of MMACHC and MMADHC, two human proteins central to intracellular vitamin B_{12} metabolism. *Mol. Genet. Metab.* **108,** 112–118
19. Kim, J., Gherasim, C., and Banerjee, R. (2008) Decyanation of vitamin B_{12} by a trafficking chaperone. *Proc. Natl. Acad. Sci. U.S.A.* **105,** 14551–14554
20. Kim, J., Hannibal, L., Gherasim, C., Jacobsen, D. W., and Banerjee, R. (2009) A human vitamin B_{12} trafficking protein uses glutathione transferase activity for processing alkylcobalamins. *J. Biol. Chem.* **284,** 33418–33424
21. Hannibal, L., DiBello, P. M., Yu, M., Miller, A., Wang, S., Willard, B., Rosenblatt, D. S., and Jacobsen, D. W. (2011) The MMACHC proteome:

hallmarks of functional cobalamin deficiency in humans. *Mol. Genet. Metab.* **103,** 226–239
22. Deme, J. C., Miousse, I. R., Plesa, M., Kim, J. C., Hancock, M. A., Mah, W., Rosenblatt, D. S., and Coulton, J. W. (2012) Structural features of recombinant MMADHC isoforms and their interactions with MMACHC, proteins of mammalian vitamin B_{12} metabolism. *Mol. Genet. Metab.* **107,** 352–362
23. Gherasim, C., Hannibal, L., Rajagopalan, D., Jacobsen, D. W., and Banerjee, R. (2013) The C-terminal domain of CblD interacts with CblC and influences intracellular cobalamin partitioning. *Biochemie* **95,** 1023–1032
24. Plesa, M., Kim, J., Paquette, S. G., Gagnon, H., Ng-Thow-Hing, C., Gibbs, B. F., Hancock, M. A., Rosenblatt, D. S., and Coulton, J. W. (2011) Interaction between MMACHC and MMADHC, two human proteins participating in intracellular vitamin B_{12} metabolism. *Mol. Genet. Metab.* **102,** 139–148
25. Stucki, M., Coelho, D., Suormala, T., Burda, P., Fowler, B., and Baumgartner, M. R. (2012) Molecular mechanisms leading to three different phenotypes in the cblD defect of intracellular cobalamin metabolism. *Hum. Mol. Genet.* **21,** 1410–1418
26. Payne, K. A., Quezada, C. P., Fisher, K., Dunstan, M. S., Collins, F. A., Sjuts, H., Levy, C., Hay, S., Rigby, S. E., and Leys, D. (2015) Reductive dehalogenase structure suggests a mechanism for B_{12}-dependent dehalogenation. *Nature* **517,** 513–516
27. Bommer, M., Kunze, C., Fesseler, J., Schubert, T., Diekert, G., and Dobbek, H. (2014) Structural basis for organohalide respiration. *Science* **346,** 455–458
28. Koutmos, M., Gherasim, C., Smith, J. L., and Banerjee, R. (2011) Structural basis of multifunctionality in a vitamin B_{12}-processing enzyme. *J. Biol. Chem.* **286,** 29780–29787
29. Otwinowski, Z., and Minor, W. (1997) Processing of x-ray diffraction data collected in oscillation mode. in *Methods in enzymology: macromolecular crystallography, part A* (Carter, C. W., and Sweet, R. M., eds), Vol. 276, pp. 307–326, Academic Press, New York
30. Adams, P. D., Afonine, P. V., Bunkóczi, G., Chen, V. B., Davis, I. W., Echols, N., Headd, J. J., Hung, L. W., Kapral, G. J., Grosse-Kunstleve, R. W., McCoy, A. J., Moriarty, N. W., Oeffner, R., Read, R. J., Richardson, D. C., Richardson, J. S., Terwilliger, T. C., and Zwart, P. H. (2010) PHENIX: a comprehensive Python-based system for macromolecular structure solution. *Acta Crystallogr. D Biol. Crystallogr.* **66,** 213–221
31. McCoy, A. J., Grosse-Kunstleve, R. W., Adams, P. D., Winn, M. D., Storoni, L. C., and Read, R. J. (2007) Phaser crystallographic software. *J. Appl. Crystallogr.* **40,** 658–674
32. Wang, J. W., Chen, J. R., Gu, Y. X., Zheng, C. D., Jiang, F., Fan, H. F., Terwilliger, T. C., and Hao, Q. (2004) SAD phasing by combination of direct methods with the SOLVE/RESOLVE procedure. *Acta Crystallogr. D Biol. Crystallogr.* **60,** 1244–1253
33. Emsley, P., Lohkamp, B., Scott, W. G., and Cowtan, K. (2010) Features and development of Coot. *Acta Crystallogr. D. Biol. Crystallogr.* **66,** 486–501
34. Murshudov, G. N., Skubák, P., Lebedev, A. A., Pannu, N. S., Steiner, R. A., Nicholls, R. A., Winn, M. D., Long, F., and Vagin, A. A. (2011) REFMAC5 for the refinement of macromolecular crystal structures. *Acta Crystallogr. D Biol. Crystallogr.* **67,** 355–367
35. Winn, M. D., Ballard, C. C., Cowtan, K. D., Dodson, E. J., Emsley, P., Evans, P. R., Keegan, R. M., Krissinel, E. B., Leslie, A. G., McCoy, A., McNicholas, S. J., Murshudov, G. N., Pannu, N. S., Potterton, E. A., Powell, H. R., Read, R. J., Vagin, A., and Wilson, K. S. (2011) Overview of the CCP4 suite and current developments. *Acta Crystallogr. D Biol. Crystallogr.* **67,** 235–242
36. Chen, V. B., Arendall, W. B., 3rd, Headd, J. J., Keedy, D. A., Immormino, R. M., Kapral, G. J., Murray, L. W., Richardson, J. S., and Richardson, D. C. (2010) MolProbity: all-atom structure validation for macromolecular crystallography. *Acta Crystallogr. D Biol. Crystallogr.* **66,** 12–21
37. DeLano, W. L. (2010) *The PyMOL Molecular Graphics System*, version 1.4, Schroedinger, LLC, New York
38. Linding, R., Jensen, L. J., Diella, F., Bork, P., Gibson, T. J., and Russell, R. B. (2003) Protein disorder prediction: implications for structural proteomics. *Structure* **11,** 1453–1459
39. Ishida, T., and Kinoshita, K. (2007) PrDOS: prediction of disordered protein regions from amino acid sequence. *Nucleic Acids Res.* **35,** W460–W464
40. Buchan, D. W., Minneci, F., Nugent, T. C., Bryson, K., and Jones, D. T. (2013) Scalable web services for the PSIPRED protein analysis workbench. *Nucleic Acids Res.* **41,** W349–W357
41. Holm, L., and Rosenström, P. (2010) Dali server: conservation mapping in 3D. *Nucleic Acids Res.* **38,** W545–W549
42. Froese, D. S., Krojer, T., Wu, X., Shrestha, R., Kiyani, W., von Delft, F., Gravel, R. A., Oppermann, U., and Yue, W. W. (2012) Structure of MMACHC reveals an arginine-rich pocket and a domain-swapped dimer for its B_{12} processing function. *Biochemistry* **51,** 5083–5090
43. Fujii, K., Galivan, J. H., and Huennekens, F. M. (1977) Activation of methionine synthase: further characterization of the flavoprotein system. *Arch. Biochem. Biophys.* **178,** 662–670
44. Wolthers, K. R., Toogood, H. S., Jowitt, T. A., Marshall, K. R., Leys, D., and Scrutton, N. S. (2007) Crystal structure and solution characterization of the activation domain of human methionine synthase. *FEBS J* **274,** 738–750
45. Drennan, C. L., Huang, S., Drummond, J. T., Matthews, R. G., and Lidwig, M. L. (1994) How a protein binds B_{12}: a 3.0 Å x-ray structure of B_{12}-binding domains of methionine synthase. *Science* **266,** 1669–1674
46. Dowling, D. P., Croft, A. K., and Drennan, C. L. (2012) Radical use of Rossmann and TIM barrel architectures for controlling coenzyme B_{12} chemistry. *Annu. Rev. Biophys.* **41,** 403–427
47. Koutmos, M., Datta, S., Pattridge, K. A., Smith, J. L., and Matthews, R. G. (2009) Insights into the reactivation of cobalamin-dependent methionine synthase. *Proc. Natl. Acad. Sci. U.S.A.* **106,** 18527–18532
48. Taga, M. E., Larsen, N. A., Howard-Jones, A. R., Walsh, C. T., and Walker, G. C. (2007) BluB cannibalizes flavin to form the lower ligand of vitamin B_{12}. *Nature* **446,** 449–453